30th International Symposium on Space Flight Dynamics (ISSFD) – AEGIS: Italy's Step Toward the Future of NEA Robotic Exploration – Rendezvous, Landing, and In-Situ Analysis

Alessandro Morselli(1,6), A. Abruscato(2), L. Deva(2), E. Valant(2), M. Cardi(2), I. Gai(1), A. Quinci(1), L. Comi(1), E. Scarpa(1), A. Locarini(1), A. Taiti(3), S. Corvatta(4), F. Bartolomasi(4), D. Santachiara(4), A. Lucchetti(5), M. Pajola(5), J. Beccarelli(5), P. Fraccaroli(5), L. Penasa(5), S. Vaghi(6), N. Michelotti(6), F. Ferrari(6), E. Gramigna(7), R. Lasagni Manghi(7), M. Zannoni(7), G. Valentini(8), A. Bigazzi(8), A. Giunta(8), M. Amoroso(8)

(1) Nautilus – Navigation in Space srl, Bologna, Italy (alessandro.morselli@spacenautilus.com)
(2) Tyvak International srl, Torino, Italy
(3) Officina Stellare, Sorcedo (VI), Italy
(4) DTM Technologies, Modena, Italy
(5) INAF – Osservatorio Astronomico di Padova, Italy
(6) Politecnico di Milano, Milano, Italy
(7) Università di Bologna, Forlì, Italy
(8) ASI – Italian Space Agency, Roma, Italy

Abstract **– AEGIS is an ASI-funded Phase A mission concept for robotic exploration of a near-Earth asteroid (NEA), developed by the AENEAS consortium. The mission targets asteroid 2002 AW, a primitive B-type potentially hazardous binary asteroid (230–380 m diameter), for rendezvous, proximity characterisation, controlled landing, and in-situ analysis. The spacecraft employs an orbiter-lander architecture based on Tyvak International's Ambassador platform with solar electric propulsion. This paper presents the flight dynamics and navigation analyses conducted during Phase A: interplanetary trajectory design and porkchop plot assessment using electric propulsion, orbit determination covariance analysis for cruise and proximity phases, proximity orbit families in the Augmented Hill Problem framework (Sun-Synchronous and Resonant Terminator Orbits), descent and landing trajectory design including Monte Carlo dispersion analysis, and radio science results for gravity field estimation.**

I. INTRODUCTION

Near-Earth asteroids (NEAs) represent both scientific archives of early Solar System material and testbeds for planetary defence and future in-situ resource utilisation (ISRU). Landmark missions (NASA's OSIRIS-REx [1], JAXA's Hayabusa2 [2], and ESA's ongoing Hera [3]) have established a foundation of knowledge on primitive rubble-pile bodies. However, no European-led mission has yet demonstrated a controlled landing on a NEA with comprehensive in-situ analysis. The Italian Space Agency (ASI) has addressed this gap by funding the AEGIS (Asteroid Exploration mission for Geophysical Investigation and in-Situ analysis) Phase A study, conducted by the AENEAS consortium comprising Nautilus, Tyvak International, Officina Stellare, and DTM, with scientific contributions from INAF – Astronomical Observatory of Padova, Politecnico di Milano, and the University of Bologna.

This paper focuses on the flight dynamics and navigation aspects of the study. The key analyses presented cover: interplanetary trajectory design using solar electric propulsion (SEP) and porkchop plot methodology; orbit determination covariance analysis for both cruise and proximity phases; proximity orbit family characterisation within the Augmented Hill Problem (AHP) framework; transfer trajectory ΔV budgeting for the approach sequence; descent and landing trajectory design including Monte Carlo dispersion; and radio science performance for gravity field estimation. Spacecraft architecture and payload are summarised in Section II to provide mission context.

II. MISSION OVERVIEW AND TARGET SELECTION

A. Mission Objectives

AEGIS addresses three strategic domains. Solar System Science: determination of bulk composition, mineralogy, surface morphology, and space weathering of a primitive NEA. ISRU and Planetary Defence: demonstration of enabling technologies for rendezvous, close proximity operations, soft landing, surface anchoring, and sub-surface sampling; and physical characterisation of a potentially hazardous binary asteroid for impact risk assessment. The engineering boundary conditions include: spacecraft wet mass ≤ 750 kg, SC-to-Sun distance within 0.75–1.44 AU, proximity operations duration ≥ 6 months, and a xenon propellant budget ≤ 73 kg for the interplanetary transfer.

B. Target Selection Methodology

Candidate targets were drawn from the JPL Horizons NEA database. A pre-filtering step retained objects with confirmed primitive or metallic taxonomy (B, C, D, T, M classes), known orbits, estimated diameters above ~100 m, and perihelion below 1.3 AU. Applying these criteria yielded a primary list of 31 well-characterised candidates and an extended list of 115 objects with confirmed orbits but limited physical data [4]. Three objects were shortlisted for detailed trade-off: 2002 AW, 1997 XR2, and 2001 TE2. The trade-off followed the ECSS-E-ST-10C Annex L methodology [5], scoring each candidate against four figures of merit: scientific and ISRU return, planetary defence relevance, programmatic flexibility (number of feasible launch windows over 2030–2040), and proximity operations feasibility (fraction of trajectories allowing ≥ 6 months of operations within communications constraints). Table 1 summarises the candidate characteristics.

Table 1: Shortlisted target asteroid characteristics

Asteroid	Class/ Type	Diam [m]	T_rot [h]	Albedo
2002 AW	B-type, PHA, Binary	230–380	4.65	0.058
1997 XR2	Xe-type, PHA	259	9.32	0.115
2001 TE2	S-type (inferred)	302	20.4	0.194

C. Selected Target: Asteroid 2002 AW

Asteroid 2002 AW emerged as the clear baseline [6]. It is a B-type potentially hazardous asteroid (the same taxonomic class as Bennu), with a primary diameter of 230–380 m, geometric albedo of 0.058, and rotation period of 4.647 hours, consistent with a rubble-pile internal structure. Uniquely, 2002 AW is a confirmed binary system: a secondary of ~50 m orbits the primary at ~520 m separation, with a revolution period of ~25.1 hours. This makes it the first primitive binary NEA that would be characterised in detail by an orbiting and landing spacecraft. As a PHA with 750 feasible departure dates across the 2030–2040 window, far exceeding 195 for 1997 XR2 and 135 for 2001 TE2, it allows an interesting launch flexibility. Key orbital parameters: semi-major axis 1.0716 AU, eccentricity 0.2567, inclination 0.574°.

D. Space Segment Overview

The AEGIS **Orbiter** is based on Tyvak International's Ambassador platform (a modular bus supporting missions up to 500+ kg) adapted for deep-space operations. The propulsion system comprises a Hall Effect Thruster (HET) operating on xenon for the interplanetary transfer, and a xenon Reaction Control System (RCS) for attitude control and proximity manoeuvres. Communications are provided by a 1.1 m X-band High Gain Antenna (HGA) for direct-to-Earth downlink, two omnidirectional Low Gain Helix Antennas (LGA) for safe-mode and proximity coverage, and an S-band inter-satellite link (ISL) for orbiter-lander relay. Deployable one-axis solar arrays and a navigation camera complete the mission-specific equipment. Estimated wet mass at Phase A closure: 593.8 kg. Table 2 summarises key parameters for both elements.

The orbiter remote-sensing payload suite comprises: a Wide-Angle Camera (WAC) and Narrow-Angle Camera (NAC) in the Vis-NIR range for shape modelling, geological mapping, and optical navigation; a Thermal Infrared (TIR) imager for thermal inertia mapping; a NIR imaging spectrometer (0.9–4 µm, off-axis Schmidt catoptric design, ~12 kg, ~261×219×102 mm³) for mineralogical mapping; and a laser altimeter (LIDAR) for ranging, shape modelling, and landing site assessment. Orbiter and payloads are shown in Fig. 1.

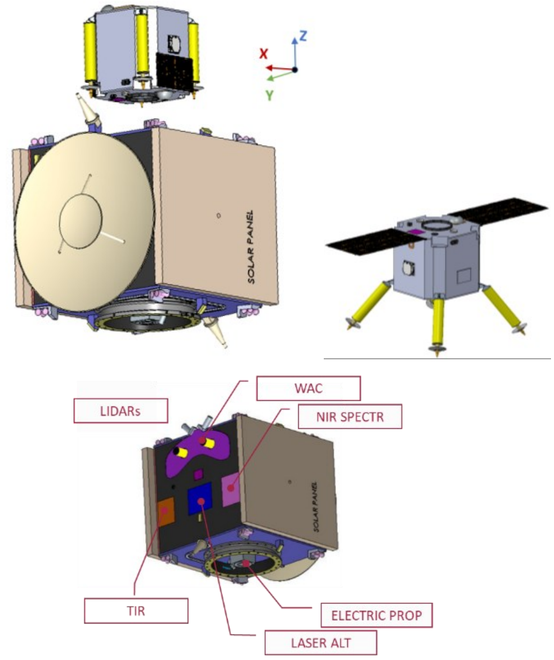

Fig. 1: Top: AEGIS Orbiter and Lander (stowed and deployed configuration). Bottom: orbiter payload suite

The AEGIS **Lander** is a purpose-built four-leg surface element designed for controlled touchdown, anchoring, and 14-day in-situ operations in the micro-gravity environment of 2002 AW. Descent attitude control and hazard avoidance are provided by cold-gas thrusters and retro-thrusters. Autonomous navigation during descent uses IMU, LIDAR, and navigation cameras. Communication with the orbiter is via the S-band ISL. Wet mass: 58.55 kg (specification: 60 kg); payload mass allocation: 14.89 kg.

Table 2: Key orbiter and lander parameters

Parameter	Orbiter	Lander
Wet mass [kg]	593.8	58.55 (max 60 kg)
Platform	Tyvak Ambassador	Four-leg custom
Propulsion	HET (Xe) + RCS	Cold-gas + retro-thrusters
Communications	X-band HGA (1.1 m) + 2×LGA	S-band ISL to orbiter
Payload mass [kg]	30 (w/o lander)	14.89
Max SC-Earth distance [AU]	1.167 (LGA) / 1.667 (HGA)	N/A

The lander payload suite (Fig. 2) includes: a panoramic camera for geological context; a microspectrometer for millimetric-scale compositional analysis; a gas chromatograph and mass spectrometer (GC-MS) for elemental and isotopic analysis; a radiometer for surface thermal characterisation; and a sampling and drilling mechanism for sub-surface material retrieval. The payload suite draws heritage from the Philae [7] and MASCOT [8] landers.

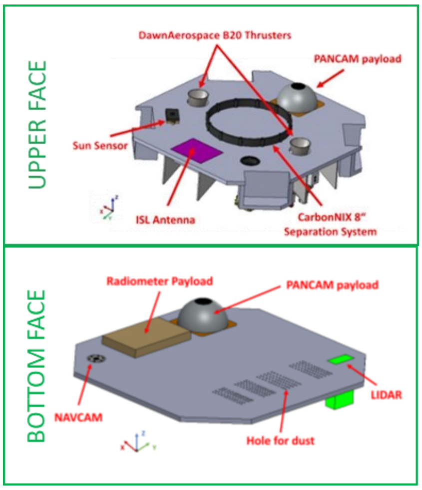

Fig. 2: AEGIS Lander payload suite

III. Interplanetary Trajectory Design

A. Electric Propulsion Transfer Analysis

Interplanetary reachability was assessed using a low-thrust trajectory optimization method based on sequential convex programming, assuming an initial spacecraft wet mass of 512 kg. A realistic model of the HET propulsion system has been implemented, with variations in maximum thrust and specific impulse depending on the input power, which in turn depends on the distance of the spacecraft from the Sun ($T_{Max} = 15 \div 60$ mN, $Isp = 1300 \div 1650$ s, $P_{in} = 200 \div 1000$ W). Porkchop plots were computed for all 31 primary candidates and the extended list of 115 backup targets across the 2030–2040 departure window, with a 15-day time discretisation. The propellant mass constraint of 73 kg defines the feasibility boundary. Of the primary-list candidates, 12 show at least one feasible launch window within the constraint; 13 require more propellant than budgeted at the assumed thrust level; 6 show no feasible direct transfers within the assumed performance envelope.

Platform constraints further filter the feasible set: SC-to-Sun distance must remain within 0.75–1.44 AU (power and thermal), and SC-to-Earth distance must not exceed 1.167 AU in the LGA-nominal scenario or 1.667 AU with the enhanced HGA configuration. Applying these filters to all porkchop plots, three rendezvous candidates survive: 2002 AW (primary), 1997 XR2 and 2001 TE2 (backups). An additional six backup targets (2008 EV5, 2001 QC34, 2006 YF, 2000 EA14, 2016 AZ65, 2006 SY5) confirm launch window coverage across the full 2030–2040 horizon, demonstrating the robustness of the mission concept across a decade of departure opportunities.

B. Launch Window Assessment

For the primary target 2002 AW, feasible electric propulsion transfers exist throughout the entire 2030–2040 departure window. The porkchop plots for the three targets are shown in Fig. 3, with red markers denoting feasibility under the LGA constraint (max SC-Earth 1.167 AU) and green markers under the HGA constraint (max 1.667 AU). The exceptional density of feasible solutions for 2002 AW (750 departure dates) is the principal driver of its selection as the baseline target. A representative optimal trajectory to 2002 AW departing in early 2030 achieves rendezvous in approximately 2033 with a propellant consumption of ~59 kg, comfortably within the 73 kg allocation.

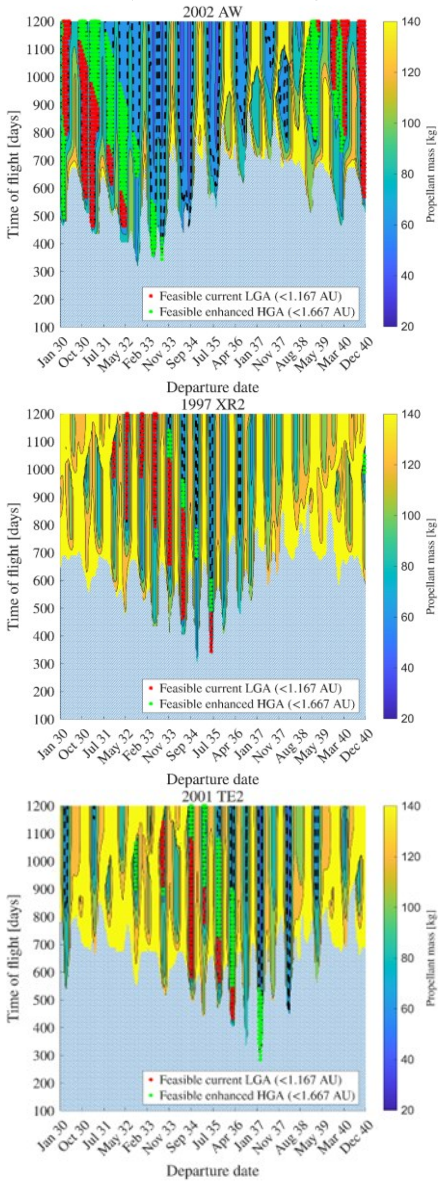

Fig. 3: Porkchop plots for primary target 2002 AW (top) and backup targets 1997 XR2 (middle) and 2001 TE2 (bottom). Red and green markers identify feasible trajectories for LGA and HGA constraints respectively.

C. *Fly-By Trajectory Optimisation*

Transfer solutions incorporating an opportunistic asteroid fly-by were evaluated to add scientific return and enable in-flight validation of optical navigation. Candidate fly-by asteroids were identified by computing the minimum distance between each NEA orbit in the filtered database and the reference transfer arc. Selection criteria required condition code = 0, perihelion > 0.75 AU, aphelion < 1.44 AU, inclination < 10°, and known estimated diameter. Asteroid 2002 BF25 emerges as the most promising candidate along several trajectories to 2002 AW, with closest approach distances as low as 0.020 AU (Time of Closest Approach: 2031-01-13). A re-optimised fuel-optimal trajectory incorporating an explicit fly-by constraint on 2002 BF25 yields: departure 2029-11-12, fly-by 2031-01-05, arrival at 2002 AW 2033-03-08, with a total propellant consumption of 59 kg, demonstrating that the fly-by is achievable with negligible additional fuel cost (Fig. 4).

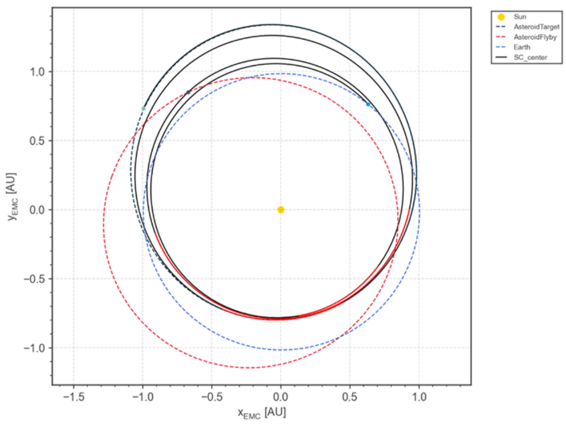

Fig. 4: Fuel-optimal interplanetary transfer to 2002 AW incorporating fly-by of asteroid 2002 BF25. Red arcs denote propelled segments.

IV. PROXIMITY OPERATIONS

A. *Dynamical Framework: Augmented Hill Problem*

Proximity trajectory design is performed within the Augmented Hill's Problem (AHP) framework, an analytical approximation of the Circular Restricted Three-Body Problem (CR3BP) valid for spacecraft in close proximity to a small body orbiting the Sun [9,10,11]. The AHP accounts for the gravitational attraction of the primary asteroid, the tidal perturbation from the Sun, and Solar Radiation Pressure (SRP). The reference epoch for proximity operations is January 2033, with the asteroid at heliocentric semi-major axis 1.0716 AU and eccentricity 0.2567. The primary gravitational parameter GM = 2.55 m^3/s^2, primary radius 190 m. The AHP is expressed in the Hill frame (x-axis Sun-to-asteroid, z-axis normal to orbital plane). SRP dominates the dynamical environment above approximately 5 km altitude at the asteroid, making SRP-leveraging trajectory design essential for orbit maintenance efficiency.

B. *Approach Phase and Characterization*

The approach sequence reduces spacecraft-target distance from 500 km (rendezvous) to 2 km (lander deployment altitude) through four transfer legs, alternated with characterization phases. Each transfer is designed as a bi-impulsive manoeuvre with optional trajectory correction manoeuvres at 7-day intervals, while characterization is performed alternating short hovering stations connected by ballistic arcs. The statistical ΔV analysis was performed over the full range of rendezvous epochs (January 2033 to April 2034) and a parametric range of transfer times for each leg. The nominal transfer times are selected to balance manoeuvre duration with fuel efficiency, exploiting SRP perturbation to reduce correction costs. The nominal ΔV values for each transfer leg are summarised in Table 3, ranging from 0.041 m/s (10→5 km) to 0.460 m/s (500→100 km). Transfer cost is minimised near the asteroid's apocenter where SRP is weakest, and is maximum for the shortest transfer times near pericenter.

C. *Orbit Families: SSTOs and RTOs*

The AHP admits two families of periodic orbits exploited during AEGIS proximity operations. Sun-Synchronous Terminator Orbits (SSTOs) are located in the asteroid's dark-side, near-parallel to the terminator plane. SRP perturbation provides the centripetal acceleration component that stabilises these orbits; stability increases with SRP strength, enabling minimal orbit maintenance. SSTOs guarantee constant illumination and intrinsic eclipse avoidance, making them ideal parking orbits and lander relay platforms. A 2 km altitude SSTO provides >70% communication coverage for landing sites above 45° latitude with a 30° minimum elevation constraint. Resonant Terminator Orbits (RTOs) bifurcate from the SSTO family through period multiplication and extend from the terminator to the light-side, offering improved mapping illumination (Sun phase angle 45–180°) and variability in target distance , thus enabling radio science opportunities. Light-side RTOs trade stability for mapping performance, requiring contingency orbit maintenance plans. Fig. 5 and Fig. 6 illustrate candidate SSTO and RTO families around 2002 AW respectively.

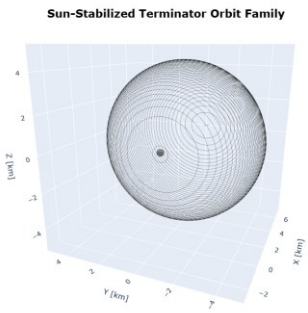

Fig. 5: Family of Sun-Synchronous Terminator Orbits (SSTOs) around 2002 AW

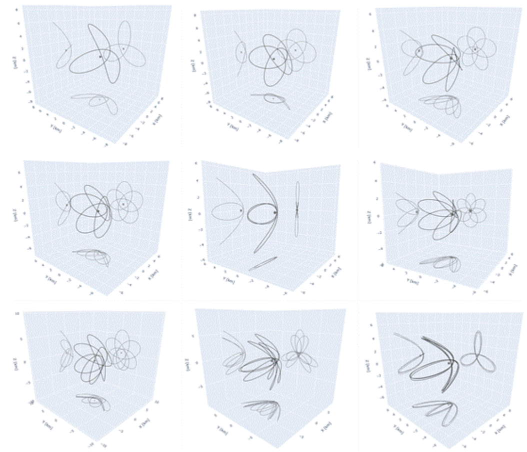

Fig. 6: Candidate light-side Resonant Terminator Orbits (RTOs) around 2002 AW.

D. Hovering Strategies

Hovering, that is maintaining a fixed position relative to the asteroid by zeroing relative velocity, is employed at multiple mission phases, following Hayabusa heritage [2,12]. A parametric ΔV analysis for 1-day hovering stations covers altitudes from 1 to 100 km at Sun phase angles from 0° to 180°. On the light-side (Sun phase < 90°), hovering cost is nearly uniform with altitude, reaching a maximum of 0.157 m/s/day at 1 km altitude and 0° Sun phase. A dark-side equilibrium point exists near 9 km altitude at 180° Sun phase, where station-keeping drops to ~0.01 mm/s/day. Hovering cost increases rapidly below 20 km altitude as the sphere of influence boundary is approached. During lander surface operations, an equatorial hovering station at 2–5 km altitude provides up to ~70% communication coverage for equatorial landing sites; for latitudes above 55° instead, an SSTO provides superior geometry.

E. Summary and ΔV budget

Table 3 presents the full baseline proximity operations sequence derived from the integrated analysis of Sections IV.B-D, covering all sub-phases from initial approach through post-landing. Transfer legs contribute modestly to the total budget; the dominant costs are the ballistic arc loop characterisation phases at 10 km, 5 km, and 1 km altitude, which collectively account for the large majority of the proximity ΔV cost. Post-landing phase values are reported as worst-case estimates.

Table 3: Proximity operations ΔV budget

Phase	ToF [days]	Altitude [km]	ΔV mean [m/s]
Approach Transfer	21	500-100	0.451
Approach Hovering	3.5	~100	0.009
Transfer 1	14	100 50	0.086
Distant Characterisation	3.5	~50	0.009
Transfer 2	7	50-10	0.135
Early Characterisation	35	~10	3.375
Transfer 3	3	10-5	0.041
Detailed Characterisation	42	~5	1.350
Transfer 4	2	5-2	0.044
Close Operations	28	~1	3.704
Landing Site Characterisation	21	~1	3.859
Landing Operations	14	2–5	0.219
Surface Operations	14	~5	0.126
Total (w/o post land)	**208**	**-**	**13.408**
Post-Landing 1 *(worst case)*	28	0.1–10	11.192
Post-Landing 2 *(worst case)*	7	~0.2	11.593
Total	**243**	**-**	**36.193**

V. DESCENT AND LANDING ANALYSIS

A. Ballistic Descent Analysis

The ballistic landing scenario is fully characterised by the release condition from the orbiter at ~2 km altitude. For a nominal anti-radial release velocity of 25 cm/s, the lander follows a near-rectilinear trajectory in the inertial asteroid equatorial frame, landing with a velocity of approximately 30 cm/s. This exceeds the 12.5 cm/s touchdown velocity requirement imposed by the anchoring and structural design. The release position latitude matches the target landing site latitude in the asteroid body-fixed frame at the landing epoch; the longitude offset accounts for asteroid rotation and the non-zero longitudinal velocity component. The release epoch is determined by integrating the landing trajectory backward from the desired touchdown state. Ballistic Monte Carlo simulations, propagating dispersions in release state and velocity, confirm that position and velocity dispersions at touchdown are large and incompatible with the precision requirement, motivating the controlled scenario.

B. Controlled Descent and Brake Manoeuvre

A single impulsive brake manoeuvre at 150 m altitude is used to reduce touchdown velocity to within the 12.5 cm/s requirement. Brake altitude selection balances touchdown precision against contingency recovery margin: lower altitudes reduce brake ΔV but leave less time to respond to off-nominal conditions; a maximum altitude exists above which zero-velocity braking is insufficient to meet the velocity requirement. At 150 m, the braking burn lasts approximately 7 minutes at the design thrust level, traversing ~80 m of vertical distance, precluding brake initiation closer to the surface. The brake impulse magnitude increases with landing longitude (orbit geometry variation), while the off-radial angle decreases toward the poles. An optional second corrective manoeuvre post-brake aligns the touchdown velocity vector with the inward surface normal, adding a few cm/s to the budget and reducing off-normal angle from ~10° to near 0°.

C. Monte Carlo Landing Dispersion

Three scenarios are assessed: ballistic, open-loop controlled, and closed-loop controlled (single and bi-impulsive). The ballistic and open-loop trajectories exhibit poor precision, with significant position dispersion at touchdown. In the closed-loop single-manoeuvre case, the differential corrector exploits the estimated lander state at brake altitude to retarget the landing site, achieving mean position error close to 0 m but a residual off-normal velocity angle of ~10°. The bi-impulsive closed-loop case achieves mean position error ≈ 0 m and mean off-normal angle ≈ 0° across all landing latitudes, with touchdown velocities within the escape velocity threshold for the primary body. Fig. 7 illustrates the position and velocity dispersion comparison across scenarios.

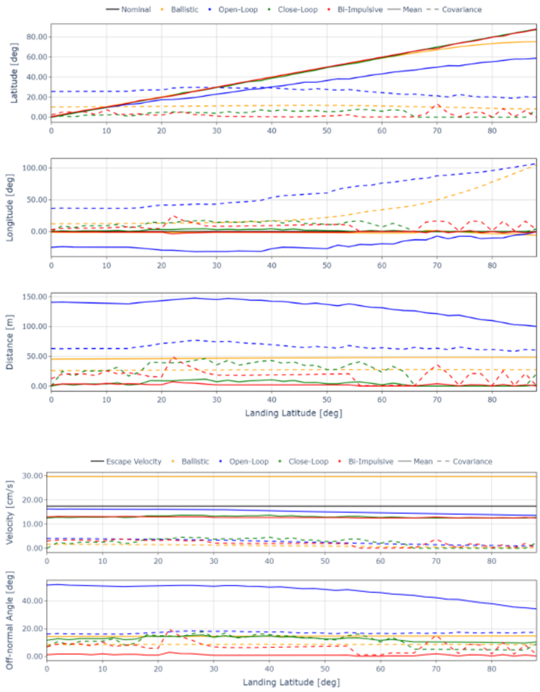

Fig. 7: Monte Carlo touchdown dispersion: ballistic, open-loop, single-manoeuvre closed-loop, and bi-impulsive closed-loop scenarios. Top: position dispersion (latitude, longitude, target distance). Bottom: velocity dispersion (magnitude and off normal angle).

The lander propellant budget associated results in a nominal 22 cm/s, corresponding to a 30 g propellant mass. Accounting for stochastic the mass increases up to 50 g. Applying a conservative 100% margin the fuel mass for the lander is only 100 g.

VI. Navigation Analysis

A. Cruise Phase Orbit Determination

A preliminary covariance analysis was performed to assess navigation accuracy across all mission phases using a batch least-squares orbit determination (OD) filter. The dynamical model includes point-mass gravity from all solar system bodies (DE440 ephemerides), relativistic corrections (Einstein–Infeld–Hoffmann), and Solar Radiation Pressure (SRP) computed from a cannonball model (initial wet mass 500 kg, cross-sectional area 4.8 m²). Stochastic accelerations accounting for unmodelled non-gravitational forces are estimated with a process noise of 1×10^{-12} km/s² per component. Estimated filter parameters include spacecraft state, reflectivity coefficient, range bias (10 m a priori), camera pointing bias (10 mdeg a priori), and stochastic accelerations. Consider parameters include station location (5 cm a priori) and tropospheric wet and dry delays (1 cm each).

Radiometric measurements consist of two-way Doppler (noise: 0.1 mm/s at 60 s integration) and range (noise: 50 m 3σ, pass-level bias). Case A evaluates the first three months of interplanetary cruise with radiometric tracking only (Fig. 8). Position uncertainty grows along-track and cross-track due to the limited angular observability of the Earth–spacecraft geometry, while velocity uncertainty stabilises owing to strong Doppler sensitivity in the radial direction. To mitigate along-track and cross-track position drift, additional angular observables (optical navigation or delta-DOR) can be introduced during cruise.

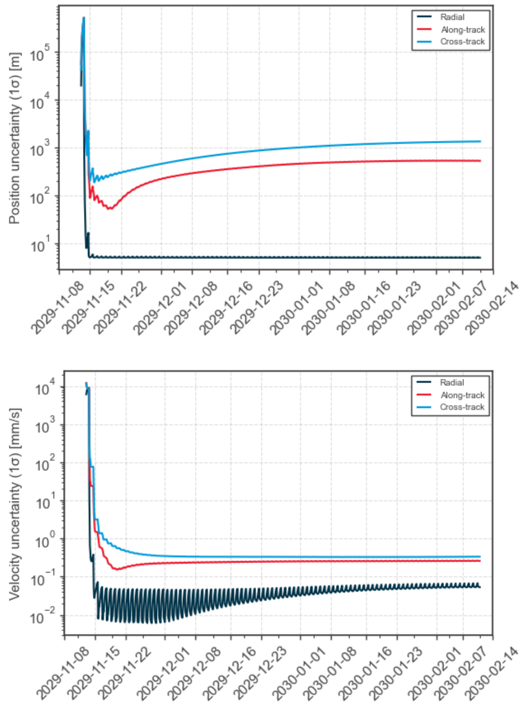

Fig. 8: State uncertainty (1σ) evolution for the first 3 months of interplanetary cruise, radiometric only.

B. Optical navigation assumptions

The optical navigation model is based on the onboard navigation camera imaging the asteroid limb. Each image provides two-line-of-sight measurements with a noise level of 2 pixels (conservative) and a pointing error of 36 arcsec a priori, consistent with parameters derived from the ESA Hera Asteroid Framing Camera heritage. During the cruise phase, periodic optical navigation campaigns can be substituted by delta-DOR measurements to mitigate along-track and cross-track position drift. During proximity operations, optical data dominate the OD solution, reducing spacecraft position knowledge relative to 2002 AW to a few metres, sufficient for safe navigation during the descent initiation phase.

C. Asteroid Proximity Navigation

Three navigation cases are analysed at asteroid proximity, progressively introducing additional measurement types and reducing altitude. Case B (500 km, radiometric only): position and velocity covariance remain comparable to the cruise case, as observability is still dominated by the Earth–spacecraft line-of-sight geometry, with limited sensitivity to lateral components. Case C (500 km, radiometric + optical): the addition of optical centroiding data reduces position uncertainty from the km-level to tens of metres (Fig. 9, top), and velocity uncertainty drops below 0.1 mm/s, demonstrating the critical contribution of geometric diversity from optical measurements to along-track and cross-track observability. Case D (50 km, radiometric + optical): position uncertainty improves further to the order of a few metres (Fig. 9, bottom); velocity components remain constrained below 0.1 mm/s. This progressive improvement from Cases B through D confirms that combined radiometric and optical navigation is essential for safe proximity operations below 50 km altitude.

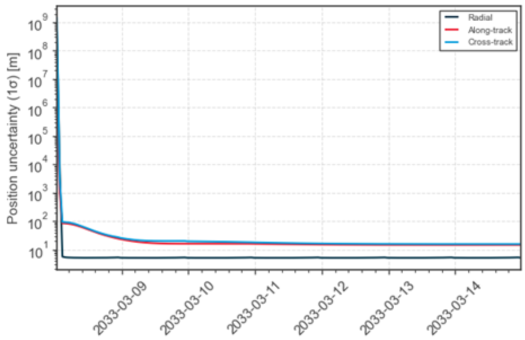

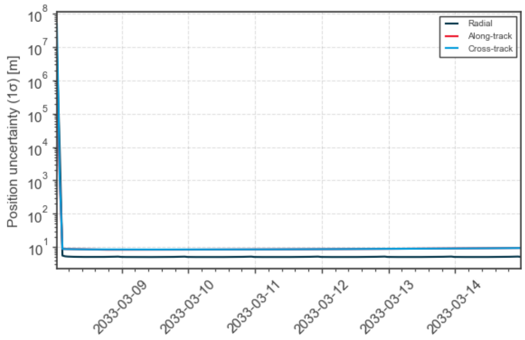

Fig. 9: Position uncertainty (1σ) evolution. Top: Case C, 500 km proximity with radiometric + optical. Bottom: Case D, 50 km proximity with radiometric + optical

VII. RADIO SCIENCE AND GRAVITY FIELD ESTIMATION

The radio science experiment exploits Earth-based radiometric tracking (two-way Doppler and range) combined with onboard optical imaging to estimate the gravitational properties of 2002 AW through OD covariance analysis performed using NASA JPL's MONTE software [13]. The dynamical model includes the heliocentric orbit of 2002 AW (orbital parameters from JPL solution 132), gravitational perturbations from all planets and 16 massive main-belt asteroids, relativistic corrections, and a Yarkovsky transverse acceleration model $a_T = A_2 r^{-2}$, with d = 2. The asteroid gravity field is modelled with spherical harmonics up to degree and order 5; coefficients are scaled from the Didymos shape model to the size of 2002 AW. Non-gravitational accelerations on AEGIS are modelled via a detailed SRP shape model, with stochastic accelerations of 5.6×10^{-12} km/s² (nominal, corresponding to 10% of SRP) and 1×10^{-11} km/s² (worst case, 24% of SRP). The expected two-way Doppler accuracy is better than 0.05 mm/s at 60 s integration, driven primarily by Earth troposphere and solar plasma contributions.

Table 4 summarises the 1σ formal uncertainties from the OD covariance analysis at the end of the close observation phase. The asteroid mass (GM) is estimated with a relative uncertainty of 0.1%, providing a highly accurate mass determination for deflection planning. The degree-2 zonal harmonic J_2 is observable from the nominal CONOPS trajectory, meeting the 50% accuracy requirement with margin (17–21% uncertainty). The degree-2 tesseral harmonic C_{22} is not observable under nominal operations, as the trajectory geometry does not provide sufficient sensitivity to the asymmetric gravity signal. Performing two low-altitude flybys during the post-close observation phase, with Earth-based range-rate measurements at closest approach over 4-hour arcs, enables C_{22} estimation at 50% relative uncertainty, in line with the desired accuracy. The Yarkovsky acceleration parameter A_2 is estimated with an uncertainty of 4.46×10^{-16} au/d², an improvement of approximately one order of magnitude relative to the current JPL ephemeris uncertainty, directly supporting long-term impact risk assessment for this PHA.

Table 4: Radio science OD covariance results (1σ formal uncertainties at end of close observation phase)

Parameter	**Nominal value**	**1σ (nom.)**	**1σ (w.c.)**
GM [km³/s²]	2.55×10^{-9}	3.29×10^{-12} [0.1%]	4.81×10^{-12} [0.2%]
J_2 [un-norm.]	7.35×10^{-2}	1.56×10^{-2} [21%]	1.73×10^{-2} [24%]
C_{22} [un-norm.]	4.47×10^{-3}	not observable*	not observable*
Yarkovsky A_2 [au/d²]	-5.16×10^{-14}	4.46×10^{-16}	4.55×10^{-16}

* C_{22} is estimated at 50% uncertainty via dedicated low-altitude flybys added to the nominal CONOPS.

VIII. CONCLUSIONS

This paper has presented the flight dynamics and navigation analyses from the AEGIS Phase A study. This is the first Italian-led concept for a comprehensive NEA robotic exploration mission. The principal results are as follows. The electric propulsion interplanetary trajectory analysis confirms mission feasibility for the primary target 2002 AW across the entire 2030–2040 departure window (750 feasible dates) within a 73 kg xenon budget, with an opportunistic fly-by of 2002 BF25 achievable at negligible propellant cost (59 kg total). The orbit determination covariance analysis demonstrates that position knowledge at 50 km proximity improves from km-level (radiometric only) to a few metres with the addition of optical navigation, confirming the adequacy of the navigation architecture for safe proximity operations. Proximity orbit design in the Augmented Hill Problem framework identifies Sun-Synchronous and Resonant Terminator Orbit families suitable for stable mapping and lander relay operations, with SSTO altitudes of 2–5 km providing >70% lander coverage at latitudes above 45°. The ΔV transfer budget for the 500 to 1 km approach sequence totals approximately 0.79 m/s deterministically, confirming proximity operations feasibility within the propellant budget. Closed-loop bi-impulsive landing trajectory control achieves near-zero position and off-normal velocity dispersion at touchdown for all landing latitudes. The radio science experiment yields GM to 0.1% uncertainty, J_2 to 17–21%, C_{22} to 50% via dedicated flybys, and Yarkovsky A_2 with a 10 time improvement over current JPL ephemeris accuracy, hence delivering scientifically significant gravity field characterisation and risk refinement for this PHA.

IX. ACKNOWLEDGEMENTS

The work described in this paper was funded by ASI under contract No. 2024-49-I.0 for "Studi di Fase A per le missioni di esplorazione robotica su asteroidi (NEA-Near Earth Asteroids)". The authors wish to acknowledge the support of the whole AEGIS consortium and the ASI team throughout the Phase A study.

X. REFERENCES

[1] D.S. Lauretta et al., "OSIRIS-REx: Sample Return from Asteroid (101955) Bennu," Space Science Reviews, vol. 212, pp. 925–984, 2017.

[2] S. Watanabe et al., "Hayabusa2 Mission Overview," Space Science Reviews, vol. 208, pp. 3–16, 2017.

[3] P. Michel et al., "The ESA Hera Mission: Detailed Characterization of the DART Impact Outcome and of the Binary Asteroid (65803) Didymos," The Planetary Science Journal, vol. 3, no. 7, p. 160, 2022.

[4] D. Perna et al., "A spectroscopic survey of the small near-Earth asteroid population: Peculiar taxonomic distribution and phase reddening," Planetary and Space Science, vol. 157, pp. 82–95, 2018.

[5] ECSS, ECSS-E-ST-10C – Space engineering: System engineering general requirements, European Cooperation for Space Standardization, 2009.

[6] C. Merrill et al., "Creating a contact binary via spacecraft impact to near-Earth binary asteroid (350751) 2002 AW," Acta Astronautica, vol. 216, pp. 334–342, 2024.

[7] J.-P. Bibring et al., "The ROSETTA Lander ('Philae') Investigations," Space Science Reviews, vol. 128, pp. 205–220, 2007.

[8] T.M. Ho et al., "MASCOT – the Mobile Asteroid Surface Scout onboard the Hayabusa2 Mission," Space Science Reviews, vol. 208, pp. 339–374, 2017.

[9] M. Giancotti et al., "Families of periodic orbits in Hill's problem with solar radiation pressure: application to Hayabusa 2," Celestial Mechanics and Dynamical Astronomy, DOI: 10.1007/s10569-014-9564-5, 2014.

[10] D.J. Scheeres, "Orbit mechanics about asteroids and comets," Journal of Guidance, Control, and Dynamics, vol. 35, no. 3, pp. 987–997, 2012.

[11] Broschart, S.B., Lantoine, G. & Grebow, D.J. Quasi-terminator orbits near primitive bodies. Celest Mech Dyn Astr 120, 195–215 (2014).

[12] T. Hashimoto, et al, "Vision-based guidance, navigation, and control of Hayabusa spacecraft – Lessons learned from real operation," IFAC Proceedings Volumes, vol. 43, no. 15, pp. 259–264, 2010.

[13] S. Evans et al., "MONTE: The next generation of mission design and navigation software," CEAS Space Journal, vol. 10, pp. 79–86, 2018.